Research Article Vol. 14, No. 9 / 1 Sep 2024 / Optical Materials Express 2114
Optical Materials EXPRESS

Transparent Ce^{3+}-doped fluorapatite (FAP) ceramics fabricated by spark plasma sintering (SPS)

Abu Yousuf,[1,2,4] Tomoya Ohno,[2] Jian Xu,[3] Takayuki Nakanishi,[1] Koji Morita,[1] Byung-Nam Kim,[1] Tohru S. Suzuki,[1] and Hiroaki Furuse[1,*]

[1]*National Institute for Materials Science (NIMS), 1-2-1 Sengen, Tsukuba, Ibaraki 305-0047, Japan*
[2]*Kitami Institute of Technology, 165 Koen-cho, Kitami, Hokkaido 090-8507, Japan*
[3]*International Center for Young Scientists (ICYS), National Institute for Materials Science (NIMS), Tsukuba 305-0044, Japan*
[4]*m3225480015@std.kitami-it.ac.jp*
[*]*FURUSE.Hiroaki@nims.go.jp*

Abstract: Polycrystalline Ce^{3+}-doped fluorapatite (Ce:FAP) transparent ceramics with fine microstructures were fabricated through liquid-phase synthesis for the initial powder and spark plasma sintering (SPS) for full densification. These ceramics were confirmed to have a single-phase crystal structure, and the average grain sizes were determined to be 139 and 135 nm for the 1 and 2 at.% Ce-doping concentrations, respectively. Their emission spectra revealed that the fabricated ceramics convert UV light to visible light emission due to the $5d \rightarrow 4f$ electronic transition of Ce^{3+}. These ceramics are expected to be useful in photonic applications.

1. Introduction

Cerium (Ce)-doped materials are widely used as phosphors in the visible wavelength range for various applications such as white LED [1,2], bio-imaging [3,4], and scintillators [5–7]. Ce^{3+} is considered as a highly suitable activator because its parity-allowed $5d$-$4f$ electron transition generates a wide spectrum of colors in the visible wavelength range with high absorption coefficient. However, the emission wavelength strongly depends on the host material, and many researchers are investigating the fabrication of efficient Ce-doped phosphor materials.

Fluorapatite ($Ca_{10}(PO_4)_6F_2$: FAP) is a fascinating host material because it exhibits excellent fluorescence properties, making it a valuable choice for laser applications [8]. Furthermore, since FAP is a prominent biomaterial, Ce-doped FAP phosphors are expected to be promising options for bio-photonic applications. In comparison to hydroxyapatite (HAP), FAP exhibits superior luminescence efficiency owing to the luminescence quenching characteristics of the OH^- group present in HAP [9]. Recent research efforts have been focused on exploring fluorapatite doped with rare earth (RE) ions such as Eu^{3+}, Sm^{3+}, Dy^{3+}, and Pr^{3+} etc. to investigate their luminescent properties [10,11].

In 2006, the emission properties of Ce:FAP powder under UV and X-ray irradiation were reported [12]. The emission spectra were recorded at a wavelength of approximately 400 nm. A similar investigation on Ce:FAP nanorods under UV excitation was conducted in 2010 [13]. The rapid decay curves observed in these studies suggest the possibility of using Ce:FAP as a scintillator material. However, to the best of our knowledge, transparent Ce:FAP materials have not yet been reported.

Typically, FAP has a hexagonal crystal structure and is not adequately transparent in polycrystalline ceramics because of grain boundary scattering due to birefringence. In such non-cubic

#530288 https://doi.org/10.1364/OME.530288
Journal © 2024 Received 4 Jun 2024; revised 11 Jul 2024; accepted 22 Jul 2024; published 2 Aug 2024

Optical Materials EXPRESS

ceramics, grain boundary scattering can be described as follows [14]:

$$\gamma(\lambda) = \frac{3\pi^2 d\Delta n^2}{2\lambda^2} \tag{1}$$

where λ is wavelength of light, d is the average grain size, and Δn represents average difference in the refractive indices at grain boundaries. One way to realize transparent ceramics for non-cubic materials is to reduce the average grain size d. We previously reported Nd:FAP, Yb:FAP, and Nd:S-FAP by controlling the grain size of the ceramics to approximately 100 nm and demonstrated their laser oscillation [15–17]. Therefore, it is expected to realize transparent Ce:FAP bulk ceramics using a process similar to that used in our previous studies.

The purpose of this study is to fabricate transparent Ce:FAP ceramics with fine microstructure for visible-light emission phosphors and to measure their emission properties, including fluorescence time decay. Ce:FAP transparent ceramics were fabricated using liquid-phase synthesis to obtain fine initial powders. Densification of the ceramics was accomplished through spark plasma sintering (SPS), which allows precise control of the sintering behavior and grain size. Additionally, their emissions in the visible wavelength region were observed under UV light excitation. Finally, we conducted lifetime measurements to evaluate their practical applicability, especially as scintillators, owing to the short fluorescence decay time observed in the previously reported Ce:FAP nano powder [13].

2. Experimental method

A schematic of the ceramic preparation process is shown in Fig. 1. A liquid-phase synthesis was used to prepare the Ce:FAP initial powder. First, Ce-doped hydroxyapatite (Ce:HAP) precursor was synthesized using $Ce(NO_3)_3.6H_2O$ (99.99%, Sigma-Aldrich), $Ca(OH)_2$ (99.9%, Kanto Chemical), and H_3PO_4 (85%, Kishida Chemical) as the raw materials. The Ce doping concentrations used were 1 and 2 at.%. Subsequently, an appropriate amount of trifluoroacetamide (CF_3CONH_2) (98%, Tokyo Chemical) was added to the Ce:HAP precursor, and the mixture was then heated to 600 °C in an electric furnace to obtain the Ce:FAP powder. The resulting powder was sieved through a screen.

A spark plasma sintering machine (LABOX-315, Sinter Land, Japan) was used to sinter the Ce:FAP powder. Initially, the powder was inserted and uniaxially pressed into a 10 mm graphite mold using a graphite punch on each side. Two circular carbon sheets were sandwiched between

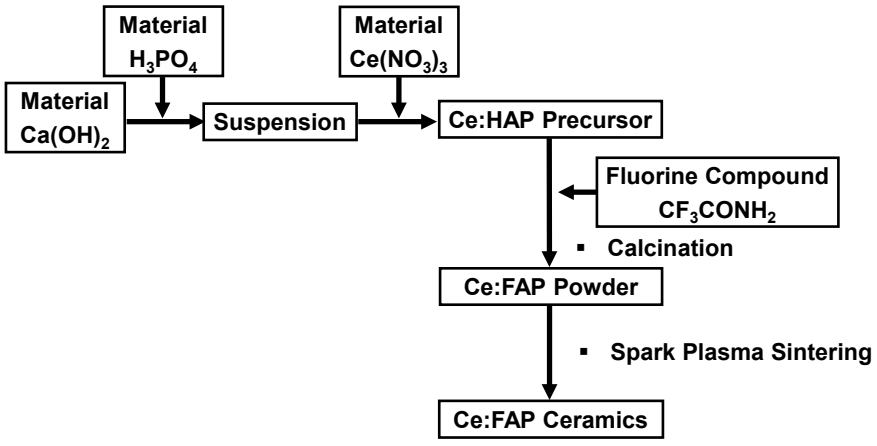

Fig. 1. Schematic diagram of fabricating of Ce:FAP ceramics.

Optical Materials EXPRESS

the Ce:FAP powder and the punches. The electrically conductive die and punches were heated at 5 °C/min heating rate under vacuum; uniaxial pressure of 80 MPa was applied to ensure that the particles get compacted during sintering. A thermocouple was used to measure the temperature of the mold; sintering temperature and holding time were maintained at 950 °C and 20 minutes, respectively. Upon completion of sintering, the ceramic surfaces were mirror polished to remove surface roughness for characterization.

The phase structure of the Ce:FAP powder and the sintered ceramics were investigated using X-ray diffraction (XRD; Ultima IV, Rigaku, Japan). The microstructural characterization of the transparent Ce:FAP ceramics was performed using field-emission scanning electron microscopy (FE-SEM; JSM-6701F, JEOL, Japan). The average grain size d was calculated from the microstructural images by analyzing the sizes with more than 500 grains, and each grain was assumed to be spherical in shape.

An UV/VIS/NIR spectrometer (UV-3600Plus, Shimadzu, Japan) was used to analyze the optical in-line transmittance spectra T; 5-mm optical aperture was used for the measurements. The total loss coefficient of the ceramics δ, including scattering and absorption coefficient, was calculated using the following equation:

$$T = (1 - R)^2 exp(-\delta t) \tag{2}$$

where t is the thickness of the samples and R represents the Fresnel loss of FAP, which is written as $R = (1\text{-}n)^2/(1 + n)^2$ and calculated using refractive index dispersion $n(\lambda)$ [18].

The photoluminescence excitation (PLE) and photoluminescence (PL) spectra, including the luminescence decay curves, were recorded using a spectrometer (FLS1000, Edinburg Instruments, UK) equipped with a xenon arc steady-state / flash lamp as the excitation source.

3. Results and discussion

3.1. Crystal structure and microstructure

Figure 2 shows the XRD patterns of the 1 and 2 at.% Ce:FAP powder and ceramic samples, respectively. The XRD diffraction peaks of the synthesized powder and fabricated ceramics were compared with the standard data in JCPDS file No. 15-0876. All the diffraction peaks of both the powders and ceramics were indexed to the pure hexagonal apatite phase of calcium fluorapatite. The peaks of the powder and ceramics are in the same position matching well with the standard card confirming the single phase of both as-prepared powder and ceramics.

However, slight discrepancies could be observed in the peak intensities of the sintered ceramics. For example, the relative peak intensities of the (002) and (112) peaks for the ceramics were smaller, whereas those of the (210) and (300) peaks were larger than those of the powder. This phenomenon was described by Watanabe et al. [19] as well as observed in our previous study [20]. During SPS, the uniaxial pressure is believed to align the c-axis of the crystal grains perpendicular to the direction of the pressure, thereby promoting anisotropic grain growth, which is reflected in the XRD pattern as changes in peak intensities (Fig. 2).

The micrographs displayed in Fig. 3(a)–(d) show FE-SEM images of both powder and ceramics. The particles of both powders were either nearly spherical or elliptical in shape at 600°C calcination temperature. The microstructural images revealed that the fabricated ceramics exhibited a dense and uniform microstructure. The average grain size d was calculated using the average cross-sectional area per grain as $S_g = (1/6)\ \pi d^2$ [14,21]. The estimated average grain sizes d of these ceramics were 139 and 135 nm, respectively, which are lower than the wavelength of visible light (380–780 nm).

3.2. Optical properties

The in-line transmittance spectra of Ce:FAP ceramics are shown in Fig. 4. The thickness of the 1 and 2 at.% Ce:FAP ceramics were 1.5 and 1.6 mm, respectively, but the in-line transmittance

Optical Materials EXPRESS

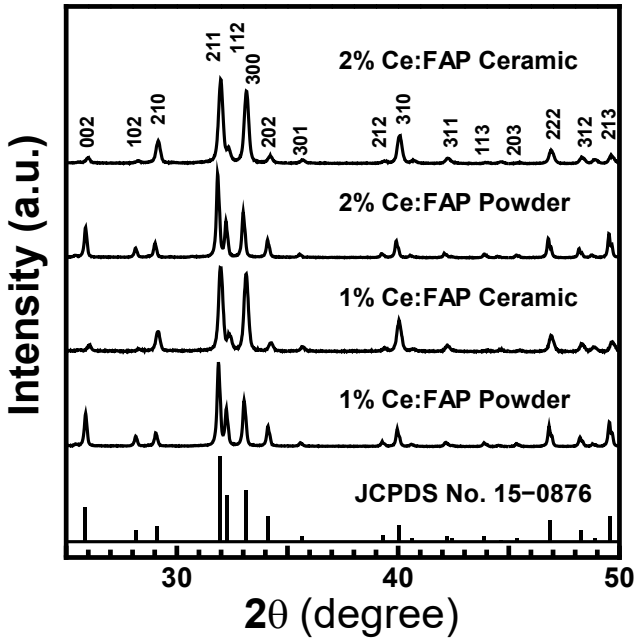

Fig. 2. XRD patterns of 1 and 2 at.% Ce:FAP powders and ceramics.

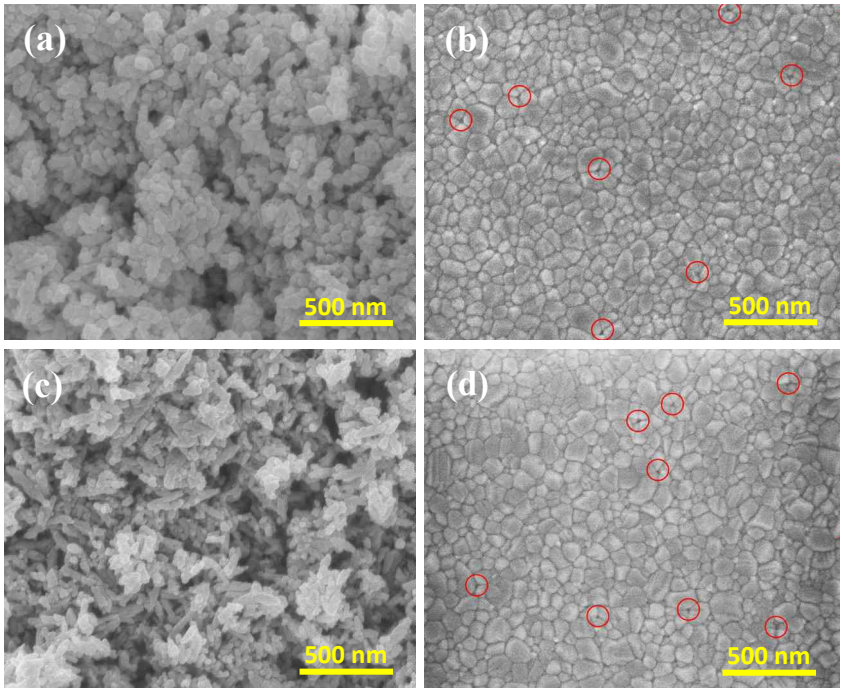

Fig. 3. FE-SEM images of (a) 1 at.% Ce:FAP powder, (b) 1 at.% Ce:FAP ceramics, (c) 2 at.% Ce:FAP powder, and (d) 2 at.% Ce:FAP ceramics. The Ce-FAP powders calcinated at 600 °C while the ceramics sintered at 950 °C temperature. The residual pores in the ceramics are indicated by red circles.

Optical Materials EXPRESS

was calculated for the 1 mm-thick ceramic from Eq. (2) to compare with our previous study [20]. The dashed black line represents the theoretical FAP transmittance calculated using the refractive-index dispersion $n(\lambda)$. The red line represents the in-line transmittance spectrum of the un-doped FAP ceramics sintered at 1000 °C measured using a thermopile obtained from Ref. [20], whose grain size is comparable with that of the Ce:FAP ceramics.

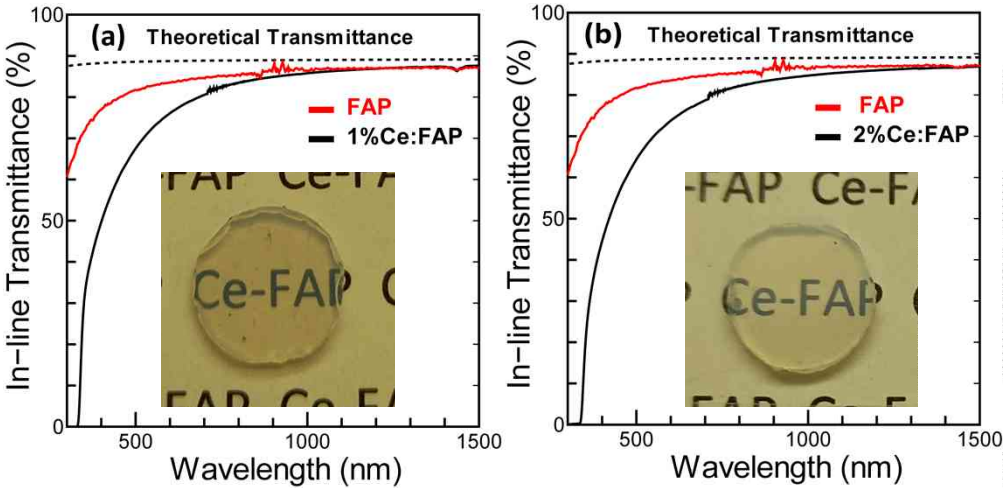

Fig. 4. In-line transmittance of (a) 1 at.% and (b) 2 at.% Ce:FAP transparent ceramics.

The Ce:FAP ceramics exhibited high transparency in the near-infrared and visible wavelength regions; however, it showed absorption bands owing to the presence of Ce^{3+} ions [22]. Figure 4 shows the in-line transmittance (> 37%) across the visible spectrum; the sudden decrease at approximately 330 nm is ascribed to Ce^{3+} ion absorption. At a wavelength of 500 nm, the in-line transmittance for the 1 and 2 at.% Ce:FAP ceramics are 67.5% and 64.4%, and the total loss coefficients are $\delta_1 = 2.7\,cm^{-1}$ and $\delta_2 = 3.2\,cm^{-1}$, respectively. The scattering coefficients due to grain boundaries were roughly determined using evaluated average grain size d and Eq. (1), resulting in $\gamma_1 = 0.91\,cm^{-1}$ and $\gamma_2 = 0.89\,cm^{-1}$ at the same wavelength. The grain-boundary scattering loss is lower for the 2 at.% ceramics owing to the smaller grain size. The discrepancy observed in the total loss coefficient could stem from Ce^{3+} absorption and the lower number of remaining pores identified in the FE-SEM image as shown in Fig. 3.

At 1000 nm wavelength, the in-line transmittances for 1 and 2 at.% Ce:FAP ceramics are 85.8% and 84.7%, respectively, which are close to theoretical transmittance. A low-temperature hot-isostatic-pressing (HIP) treatment may be effective to eliminate residual pores and further increase the transmittance [23].

3.3. Fluorescent properties

The Ce^{3+} ion possessing a $4f^1$ site can function as an effective emission center due to the parity and spin-allowed $4f$-$5d$ transitions. The PLE/PL of the 1 and 2 at.% Ce:FAP ceramics, including their decay curves, are shown in Fig. 5. The excitation spectra in Fig. 5(a) consist of a broad wavelength range of 240–400 nm, obtained by monitoring the emission at 413 nm. The strongest band was detected with a maximum peak at 310 nm accompanied by a less intense shoulder band at 292 nm. The excitation peaks represent the transitions from the ground state $^2F_{5/2}$ and $^2F_{7/2}$ of Ce^{3+} to the excited $5d$ states [24,25].

In Fig. 5(a), the ceramic emission spectra encompass the 350–700 nm range with an intense emission centered at 413 nm under 310 nm excitation wavelength. The emission is induced by the

Optical Materials EXPRESS

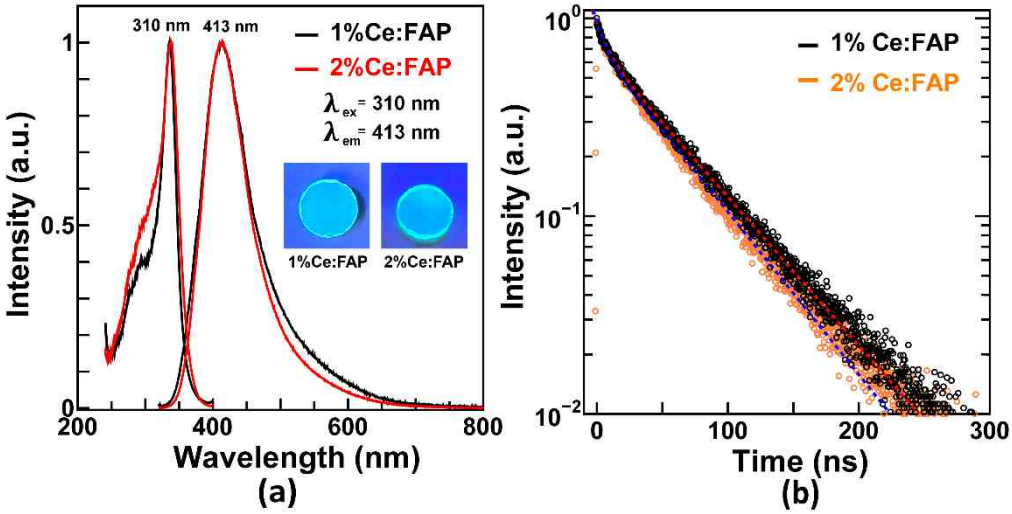

Fig. 5. PLE and PL spectra of (a) 1 and 2 at.% Ce:FAP ceramics (λ_{ex} = 310 nm, λ_{em} = 413 nm) and (b) temporal decay curve of 1 and 2 at.% Ce:FAP ceramic samples. Inset images in Fig. 5(a) correspond to luminescence of the ceramics under UV light excitation (370 nm) observed in the dark.

inter-configurational 5*d*→4*f* transition from the excited 5*d* state to the ground state of Ce^{3+} ions [26]. The inset images correspond to the luminescence of the ceramics under UV light excitation (370 nm) observed in the dark. The images confirm the emission of light from both ceramics.

The Ce^{3+} ions exhibited a broad emission spectrum, indicating emission via multiple transitions. FAP hosts contain two calcium cations referred to as Ca^{2+} (I) and Ca^{2+} (II). Gaft *et al.* revealed that Ce^{3+} ions could replace both the Ca^{2+} (I) and Ca^{2+} (II) sites [27], and Yang *et al.* demonstrated the presence of an excitation band at approximately 296 nm [28]. The PL properties of Ce^{3+}-doped FAP at various concentrations have been extensively discussed by Zeng *et al.* [12]. In addition, they indicated that Ce^{3+} ions occupy Ca^{2+} (II) and Ca^{2+} (I) sites at 292 and 313 nm excitation wavelengths, respectively. This result suggests that the Ce^{3+} ions are primarily located at the Ca^{2+} (I) sites in our ceramic samples because only the 310 nm peak is visible in the excitation spectrum shown in Fig. 5(a).

The luminescence decay curves of the 1 and 2 at.% Ce:FAP ceramics were obtained at wavelength of 430 nm under laser excitation at 375 nm (Fig. 5(b)). These curves were fitted to a double exponential function as $I(t) = A_1\exp(-t/\tau_1)+A_2\exp(-t/\tau_2)$. The average lifetimes of the 1 and 2 at.% Ce:FAP ceramics were determined to be 58 and 51 ns, respectively, using the following equation [29]:

$$\tau = (A_1\tau_1^2 + A_2\tau_2^2)/(A_1\tau_1 + A_2\tau_2) \quad (3)$$

The short lifetime of the 1 at.% and 2 at.% Ce:FAP ceramic can be attributed to the allowed character of the Ce^{3+} ion 5*d*–4*f* transition. Additionally, an increased Ce doping concentration decreased the ceramic's lifetime. Such behavior is consistent with previous studies on Ce-doped apatite [30].

To investigate the feasibility of using this material as a scintillator, we will try to measure its fluorescence properties under X-ray irradiation in the future. Although no significant difference has been observed between the fluorescence properties for the 1 and 2 at.% Ce concentrations in this study, detailed concentration-dependent analyses will also be conducted at higher concentrations to gain further insights into the Ce-occupied sites and fluorescent mechanisms.

Optical Materials EXPRESS

4. Conclusion

We successfully fabricated 1 and 2 at.% Ce:FAP transparent ceramics via liquid-phase synthesis and spark plasma sintering. The low SPS temperature of 950 °C effectively suppressed grain growth and grain boundary scattering, and the corresponding treated ceramics exhibited an optical transparency > 64% at a wavelength of 500 nm. The excitation spectrum of Ce-doped FAP exhibited a broad peak centered at approximately 310 nm, whereas the emission spectrum displayed a broad band covering the entire blue emission spectrum. Overall, the Ce:FAP transparent ceramics exhibit a high transparency at visible wavelengths, and owing to their emission properties and relatively short lifetimes, these materials has the possibility to utilize in photonic applications.

Funding. Fusion Oriented REsearch for disruptive Science and Technology (JPMJFR203S); Japan Society for the Promotion of Science (21H01611, 23K21035).

Acknowledgment. Portions of this work were presented at Laser Congress 2023 (ASSL, LAC), Technical Digest Series (Optica Publishing Group), paper JW2A.2

Disclosures. The authors declare no conflicts of interest.

Data availability. The data underlying the results presented in this paper are not publicly available at this time but may be obtained from the authors upon reasonable request.

References

1. S. Nishiura, S. Tanabe, K. Fujioka, *et al.*, "Properties of transparent Ce:YAG ceramic phosphors for white LED," Opt. Mater. **33**(5), 688–691 (2011).
2. V. Tucureanu, A. Matei, and A. M. Avram, "Synthesis and characterization of YAG:Ce phosphors for white LEDs," Opto-Electron. Rev. **23**(4), 239–251 (2015).
3. B. Liu, X. Duan, and Y. Yi, "Improved light extraction efficiency of cerium-doped biomedical imaging scintillator by monolayers of periodic arrays of polystyrene spheres," Mater. Res. Soc. Symp. Proc. **1627**(1), mrsf13-1627-l09-98 (2014).
4. W. Huang, Z. Mao, L. Chen, *et al.*, "Synthesis and characterisation of fluorescent and biocompatible hydroxyapatite nanoparticles with cerium doping," Micro Nano Lett. **13**(5), 699–703 (2018).
5. M. Mori, J. Xu, G. Okada, *et al.*, "Comparative study of optical and scintillation properties of Ce:YAGG, Ce:GAGG and Ce:LuAGG transparent ceramics," J. Ceram. Soc. Jpn. **124**(5), 569–573 (2016).
6. Y. Takebuchi, K. Watanabe, D. Nakauchi, *et al.*, "Scintillation properties of Ce-doped $LiAlO_2$ for neutron detection," J. Ceram. Soc. Jpn. **129**(7), 20233397 (2021).
7. A. Lempicki and J. Glodo, "Ce-doped scintillators: LSO and LuAP," Nucl. Instr. and Meth. in Phys. Res. A **416**(2-3), 333–344 (1998).
8. S. A. Payne, L. D. Deloach, L. K. Smith, *et al.*, "Ytterbium-doped apatite-structure crystals: A new class of laser materials," J. Appl. Phys. **76**(1), 497–503 (1994).
9. A. V. Paduraru, A. M. Musuc, O. C. Oprea, *et al.*, "Synthesis and characterization of photoluminescent Ce(III) and Ce(IV) substituted hydroxyapatite nanomaterials by co-precipitation method: Cytotoxicity and biocompatibility evaluation," Nanomaterials **11**(8), 1911 (2021).
10. D. V. Milojkov, O. S. Silvestre, S. D. Vojislav, *et al.*, "Fabrication and characterization of luminescent Pr^{3+} doped fluorapatite nanocrystals as bioimaging contrast agents," J. Lumin. **217**, 116757 (2020).
11. B. Demir and E. Ayas, "Effects of sintering temperature and doping content on luminescence properties of rare earth (Sm^{3+}, Eu^{3+}, and Dy^{3+}) doped natural fluorapatite," J. Solid State Chem. **306**, 122783 (2022).
12. Q. Zeng, H. Liang, G. Zhang, *et al.*, "Luminescence of Ce^{3+} activated fluoro-apatites $M_5(PO_4)_3F$ (M ≤ Ca, Sr, Ba) under VUV-UV and X-ray excitation," J. Phys.: Condens. Matter **18**(42), 9549–9560 (2006).
13. C. Zhang, S. Huang, D. Yang, *et al.*, "Tunable luminescence in Ce^{3+}, Mn^{2+} -codoped calcium fluorapatite through combining emissions and modulation of excitation: A novel strategy to white light emission," J. Mater. Chem. **20**(32), 6674–6680 (2010).
14. R. Apetz and M. P. B. Van Bruggen, "Transparent alumina : a light-scattering model," J. Am. Ceram. Soc. **86**(3), 480–486 (2003).
15. H. Furuse, N. Horiuchi, and B. N. Kim, "Transparent non-cubic laser ceramics with fine microstructure," Sci. Rep. **9**(1), 10300 (2019).
16. H. Furuse, T. Okabe, H. Shirato, *et al.*, "High-optical-quality non-cubic Yb^{3+} -doped $Ca_{10}(PO_4)_6F_2$ (Yb:FAP) laser ceramics," Opt. Mater. Express **11**(6), 1756 (2021).
17. H. Furuse, Y. Mochizuki, D. Kato, *et al.*, "Strontium fluorapatite (S-FAP) nano-grained laser ceramics," Scr. Mater. **241**, 115881 (2024).
18. P. Becker, E. Libowitzky, R. Kleinschrodt, *et al.*, "Linear optical properties and Raman spectroscopy of natural fluorapatite," Cryst. Res. Technol. **51**(4), 282–289 (2016).

Optical Materials EXPRESS

19. Y. Watanabe, T. Ikoma, A. Monkawa, *et al.*, "Fabrication of transparent hydroxyapatite sintered body with high crystal orientation by pulse electric current sintering," J. Am. Ceram. Soc. **88**(1), 243–245 (2005).
20. H. Furuse, D. Kato, K. Morita, *et al.*, "Characterization of transparent fluorapatite ceramics fabricated by spark plasma sintering," Materials **15**(22), 8157 (2022).
21. H. Furuse, S. Nakasawa, H. Yoshida, *et al.*, "Transparent ultrafine Yb^{3+}:Y_2O_3 laser ceramics fabricated by spark plasma sintering," J. Am. Ceram. Soc. **101**(2), 694–702 (2018).
22. A. Yousuf, Y. Mochizuki, S. Hirai, *et al.*, "Fluorescence and optical properties of Er and Ce doped fluorapatite (FAP) transparent ceramics," in *Laser Congress 2023 (ASSL, LAC), Technical Digest Series* (Optica Publishing Group), paper JW2A.2 (2023).
23. S. Cohen, B. Ratzker, M. Solol, *et al.*, "Polycrystalline transparent magnesium aluminate spinel processed by a combination of spark plasma sintering (SPS) and hot isostatic pressing (HIP)," J. Eur. Ceram. Soc. **38**(15), 5153–5159 (2018).
24. Z. L. Wang, Z. W. Quan, P. Y. Jia, *et al.*, "A facile synthesis and photoluminescent properties of redispersible CeF_3, CeF_3:Tb^{3+}, and CeF_3:Tb^{3+}/LaF_3 (core/shell) nanoparticles," Chem. Mater. **18**(8), 2030–2037 (2006).
25. A. Gektin, N. Shiran, V. Nesterkina, *et al.*, "Luminescence of heavily Ce-doped alkaline-earth fluorides," J. Lumin. **129**(12), 1538–1541 (2009).
26. M. Xie, Y. Huang, Y. Tao, *et al.*, "Improving the BAM VUV-Irradiation Degradation with a UV-Blue Emitting Phosphor CLPF-Tm," J. Electrochem. Soc. **157**(11), J401–J404 (2010).
27. M. Gaft, G. Panczer, R. Reisfeld, *et al.*, "Laser-induced time-resolved luminescence as a tool for rare-earth element identification in minerals," Phys. Chem. Miner. **28**(5), 347–363 (2001).
28. P. Yang, G. Q. Yao, and J. H. Lin, "Photoluminescence of Ce^{3+} in haloapatites $Ca_5(PO_4)_3$ X," Inorg. Chem. Commun. **7**(2), 302–304 (2004).
29. A. Sillen and Y. Engelborghs, "The correct use of 'average' fluorescence parameters," Photochem. Photobiol. **67**(5), 475–486 (1998).
30. I. E. Kolesnikov, A. M. Nikolaev, E. Lähderanta, *et al.*, "Structural and luminescence properties of Ce^{3+} -doped hydroxyapatite nanocrystalline powders," Opt. Mater. **99**, 109550 (2020).